Optically detected magnetic resonance study of an arsenic-antisite–arsenic-vacancy complex in GaAs

F. K. Koschnick, K.-H. Wietzke, and J.-M. Spaeth
Department of Physics, University of Paderborn, 33095 Paderborn, Germany
(Received 9 March 1998; revised manuscript received 6 May 1998)

An arsenic-antisite-related defect produced in *n*-type GaAs by 2 MeV electron irradiation was investigated using magnetic circular dichroism of the optical absorption (MCDA), MCDA-detected electron paramagnetic resonance (MCDA-EPR), and MCDA-detected electron-nuclear double resonance (MCDA-ENDOR). In comparison to several other arsenic-antisite-related defects, like the $EL2$ defect, the investigated defect has a reduced hyperfine interaction with the central As_{Ga} atom (2050 MHz compared to 2650 MHz for $EL2$). Large superhyperfine interactions with the nearest arsenic neighbor shell of the order of 250 MHz were observed. From the analysis of the MCDA-EPR line shape and the MCDA-ENDOR data, it was concluded that the defect consists of an arsenic antisite and a first As shell vacancy. [S0163-1829(98)06536-9]

I. INTRODUCTION

GaAs is one of the most used semiconductor materials. Its direct band gap and high electron mobility lead to many applications where high speed or IR light are involved, e.g., fast digital circuits and laser diodes. The electrical and optical properties of GaAs are influenced by intrinsic defects. The most prominent intrinsic defect in GaAs is the $EL2$ defect, a deep arsenic-antisite–related (As_{Ga}-related) double donor, which is responsible for the semi-insulating (SI) character of nominally undoped, as-grown GaAs. By irradiation with high-energy electrons intrinsic defects like As_{Ga}-related defects can be artificially produced in concentrations that allow their investigation using magnetic resonance techniques, such as the magnetic circular dichroism of the optical absorption (MCDA), MCDA-detected electron paramagnetic resonance (MCDA-EPR), and MCDA-detected electron-nuclear double resonance (MCDA-ENDOR).

A whole family of As_{Ga}-related defects has been identified.[1] Besides the $EL2$ at least three other As_{Ga}-related defects are formed by electron irradiation of GaAs. Two of them were attributed to the isolated As_{Ga} defect and an antistructure pair [As_{Ga}-Ga_{As} (nnn), i.e., an As_{Ga} with a Ga antisite (Ga_{As}) in the next-nearest-neighbor position].[1] The EPR spectra of all three of those defects have ^{75}As hyperfine (hf) splittings almost undistinguishable from the hf structure of the $EL2$.[1] In contrast, the so-called As_{Ga}-X_2 defect,[2,3] a defect, which is produced by electron irradiation at room temperature in *n*-type GaAs, has a reduced hf splitting compared to the other three As_{Ga}-related defects mentioned above. The As_{Ga}-X_2 has an ionization level at 1.2 eV above the valence-band edge.[3,4] Its introduction rate is relatively large ($1\ cm^{-1}$). Investigations using different electron irradiation fluences and dopants suggest that the As_{Ga}-X_2 defect is an intrinsic defect without extrinsic constituents.[5] Tentatively, the model of an As_{Ga}-related defect with a nearest As vacancy (V_{As}) was proposed by Bardeleben, Bourgoin, and Moret,[3] who performed conventional EPR measurements. Later, the same first author with others proposed the model of an isolated, but distorted As antisite defect with a broken bond and hence it was negatively charged.[6]

However, from EPR alone it was not possible to analyze the detailed microscopic structure of the defect. The high abundance of magnetic isotopes with a nuclear spin of $I=3/2$ of both lattice atoms in GaAs causes a large inhomogeneous broadening of the hf-split EPR lines preventing the resolution of the superhyperfine (shf) interactions, i.e., the magnetic interactions between the unpaired electron spin and the nuclear spins of the neighbor nuclei. The resolution of the shf interactions is needed to establish a microscopic model.[7] ENDOR measurements can resolve these shf interactions. We performed MCDA-detected ENDOR measurements that are more sensitive than conventional ENDOR, which was not successful for sensitivity reasons.[7] As a result of our determination of the shf interactions and their analysis, we propose that the As_{Ga}-X_2 defect is a complex defect consisting of an arsenic antisite with a vacancy in the first arsenic shell (As_{Ga}-V_{As}).

II. EXPERIMENTAL DETAILS

We used Te-doped liquid encapsulated Czochralski (LEC) GaAs with a *n*-type carrier concentration of $n=3.4\times10^{17}\ cm^{-3}$ at room temperature. The sample was irradiated at 4.5 K with 2 MeV electrons at the Forschungszentrum Jülich. The irradiation fluence was $1\times10^{17}\ e^{-}\ cm^{-2}$. The irradiation fluence did not suffice to lower the Fermi level to a midgap position. After warming the crystal to room temperature, the As_{Ga}-X_2 defect was observed. The defect can also be produced by electron irradiation at room temperature.[3]

The MCDA, which is the differential absorption of left and right circularly polarized light propagating along an external magnetic field, was determined with a linear polarizer in combination with an optical stress modulator via a lock-in technique. MCDA, MCDA-EPR, and MCDA-ENDOR measurements were performed using a computer-controlled, custom-built *K*-band spectrometer ($\nu=24$ GHz). MCDA-EPR was detected as a microwave-induced change of the MCDA. MCDA-ENDOR was measured as an increase of the MCDA-EPR signal due to nuclear magnetic resonance

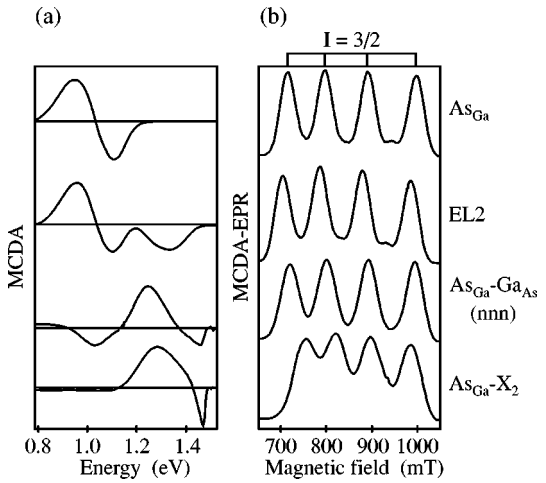

FIG. 1. (a) MCDA spectra and (b) MCDA-detected *K*-band EPR (MCDA-EPR) spectra of four different As_{Ga}-related defects. The spectra of the four different arsenic antisite-related defects were recorded in different GaAs samples (see text). The hf splitting of the As_{Ga}-X_2 defect is reduced by about 25% compared to the other ''large'' As antisite hf splittings. The measurement temperatures were 1.5 K. The microwave power was chosen to be -20 dBm to avoid saturation broadening (0 dBm=1 mW).

(NMR) transitions induced simultaneously with the EPR transitions by a radio frequency source. A cooled germanium detector was used to measure the transmitted light. For further experimental details the reader is referred to Ref. 7.

III. EXPERIMENTAL RESULTS

A. MCDA-EPR measurements

Figure 1 shows the MCDA (a) and MCDA-EPR spectra (b) of the four different arsenic-antisite–related defects [As_{Ga}, $EL2$, As_{Ga}-Ga_{As} (nnn), and As_{Ga}-X_2]. The four different defects were measured in samples with different preparation conditions. The As_{Ga} defect was measured in SI GaAs, which was irradiated with 2 MeV electrons at 4.2 K and kept below 77 K. The $EL2$ defect was measured in as-grown SI GaAs. The As_{Ga}-Ga_{As} (nnn) defect was observed in SI GaAs which was electron irradiated at 4.2 K and warmed to room temperature, and the As_{Ga}-X_2 defect was measured in Te-doped, electron-irradiated GaAs as described above. As is the case for the other arsenic-antisite–related defects having the ''large'' hf interaction, the MCDA-EPR spectrum of the As_{Ga}-X_2 defect [see Fig. 1(b)] yields little structural information. Within experimental error all the MCDA-EPR spectra of Fig. 1(b) are isotropic. The first three defects have almost undistinguishable MCDA-EPR spectra as clearly seen in Fig. 1(b). However, the As_{Ga}-X_2 defect differs from the others. The MCDA-EPR spectrum has four hf lines with about equal intensity and width. From this it is inferred that the defect has an ^{75}As as a central nucleus (nuclear spin $I=3/2$ and 100% abundance). A Ga central nucleus cannot explain the MCDA-EPR spectrum. [Ga has two isotopes: ^{69}Ga (60.1%) and ^{71}Ga (39.9%), each with $I=3/2$, but with different nuclear g factors.] However, the MCDA-EPR spectrum alone cannot be used to determine whether the defect involves an As antisite or an As interstitial.

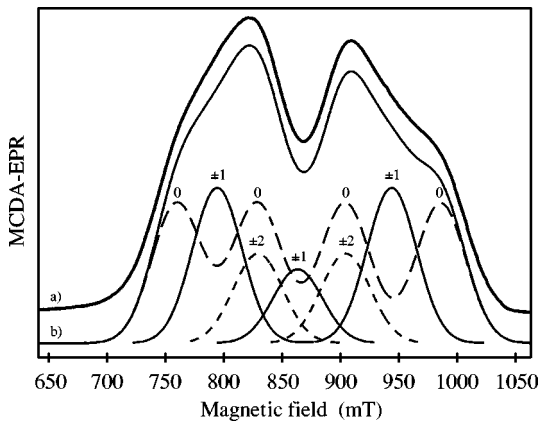

FIG. 2. Trace *a*: MCDA-EPR spectrum recorded under saturation conditions with a microwave power of 18 dBm (0 dBm=1 mW) at 1.287 eV, $T=1.5$ K, and microwave frequency 24.08 GHz. The measured spectrum was calculated with excellent agreement (trace *b*) as a sum of the three less intense spectra. These spectra were calculated assuming Gaussian lines and allowed transitions ($\Delta m_S=\pm1$, $\Delta m_I=0$, dashed four-line spectrum marked with 0) and forbidden transitions ($\Delta m_S=\pm1$, $\Delta m_I=\pm1$, solid three-line spectrum marked with ±1), and ($\Delta m_S=\pm1$, $\Delta m_I=\pm2$, dashed lines at the field positions of two of the allowed lines in the middle of the spectrum marked with ±2). The inner $\Delta m_S=\pm1$, $\Delta m_I=\pm1$ line has a smaller amplitude than the two outer ones.

The microwave power dependence of the MCDA-EPR spectrum was studied. ''Forbidden'' transitions arose with increased microwave power. These transitions are not seen in Fig. 1(b) which was taken at low power (-20 dBm). An MCDA-EPR spectrum recorded with a microwave power of 18 dBm (0 dBm=1 mW) incident on the cavity, the highest power available in our MCDA-EPR/ENDOR spectrometer, is shown as trace *a* in Fig. 2. A double humped ''camel'' spectrum was found. Detailed calculations were made to try and explain this spectral shape.

The MCDA-EPR spectral changes with microwave power cannot be explained with the usual time-dependent, second-order perturbation theory, since in second order, the forbidden transitions would be smaller than the allowed ones by a factor of B_1^2/B_0^2 (where B_1 is the oscillating magnetic-field amplitude of the microwaves and B_0 is the static magnetic field). In our experiments this factor is of the order of 10^{-10} for the maximum microwave power available. It will be shown below that the observation of forbidden transitions is caused by the saturation of the spin system with high microwave power. In MCDA-EPR, it is necessary to drive the investigated spin system away from thermal equilibrium, favorably into saturation to substantially change the spin population of the Zeeman levels of the defect ground state. Otherwise, one cannot observe a change of the MCDA due to an EPR transition (see e.g., Ref. 7).

In Fig. 2 the long-dashed line shows the four hf lines whose peaks are labeled with 0. Forbidden lines with $\Delta m_I=\pm1$ would be located in the middle between the allowed hf lines (see Fig. 2). Forbidden lines with $\Delta m_I=\pm2$ would be superimposed on the two allowed hf lines in the middle of the spectrum (see weak short-dashed lines in Fig. 2). Possible reasons for forbidden EPR transitions are a quadrupole

TABLE I. Relative amplitudes of the allowed and forbidden MCDA-EPR transitions for different microwave powers (for 18 dBm, see Fig. 2). In the line shape fitting to the spectra only the relative amplitudes of the allowed and forbidden transitions were varied. The positions and widths of the lines were set in advance. The lowest row in the table was calculated using Eq. (3) and the parameters c_1 and c_2 that were obtained from a fit of Eq. (3) to the measured relative intensities at 18 dBm, -2 dBm, and -12 dBm. The power of -48 dBm was chosen because then no saturation occurs and the relative intensities of the allowed transitions was exactly one. Therefore, the lowest line in the table gives the relative transition probabilities for the respective forbidden transitions in comparison to the allowed ones.

Microwave power	$\Delta m_I=0$	$\Delta m_I=\pm1$ (outer lines)	$\Delta m_I=\pm1$ (central line)	$\Delta m_I=\pm2$
18 dBm	3000	3700	1700	2300
-2 dBm	2800	900	500	400
-12 dBm	1700	200	150	0
-48 dBm	1.0	0.030	0.016	0.012

interaction of the central nucleus, anisotropies of the g tensor and/or the hf tensor, and/or large shf interactions. The anisotropies or large shf interactions cause a deviation of the quantization axis of the electron spin from the magnetic-field direction if it is not parallel to the principal axes of both tensors. In such a case the three forbidden $\Delta m_I=\pm1$ transitions would occur with equal intensities. On the other hand, the forbidden $\Delta m_I=\pm1$ transitions would not have equal intensities in the case of a quadrupole interaction. A suppression of the inner forbidden line is typical for forbidden transitions caused by a quadrupole interaction. For a system with an isotropic g factor, an isotropic hf interaction, and a quadrupole interaction, the relative intensity of the forbidden lines with $\Delta m_S=\pm1$ and $\Delta m_I=\pm1$ can be calculated with the following expression:[8]

$$\frac{\mathrm{Int}_{\pm}}{\mathrm{Int}_0}=\left\{\frac{2q\,\cos\beta\,\sin\beta}{a m_S(m_S-1)}\right\}^2\times m_q^2\{(I+\tfrac{1}{2})^2-m_q^2\},\qquad(1)$$

in which $\mathrm{Int}_{\pm}$ are the intensities of the forbidden $\Delta m_S=\pm1$ and $\Delta m_I=\pm1$ transitions, Int_0 is the intensity of the allowed $\Delta m_S=\pm1$ and $\Delta m_I=0$ transitions, a is the isotropic hf interaction parameter, q is the quadrupole interaction parameter, β is the angle between the z axis of the quadrupole tensor and the magnetic field B_0, m_S is the spin quantum number of the electron, and m_q is the average of the two nuclear spin quantum numbers involved in the transition $[(m_I+m_I')/2]$. The relation of the hf and quadrupole parameters to the respective tensors are explained in Sec. III B; see also, e.g., Refs. 7 and 8. The quantum number m_q is zero for the forbidden transition with $m_I=1/2\rightarrow m_I'=-1/2$. Therefore, this transition that corresponds to the central line of the three forbidden lines with $\Delta m_I=\pm1$ is suppressed. The intensity of the forbidden lines with $\Delta m_I=\pm2$ due to quadrupole effects is one order of magnitude smaller than those of the $\Delta m_I=\pm1$ lines.[8]

Assuming allowed and forbidden transitions and Gaussian lines of equal width for the transitions, it is possible to try and synthesize the observed spectra. The relative amplitudes of the allowed and forbidden MCDA-EPR transitions for different microwave powers (18 dBm, -2 dBm, and -12 dBm) were determined with a least-squares fit to the measured spectra. In the line shape fitting the positions and widths of the lines of the individual transitions were set in advance. Table I shows the results for MCDA-EPR spectra recorded with different microwave powers. Figure 2 shows for a microwave power of 18 dBm the individual spectra and their sum [trace (b)].

The stationary population difference $\Delta n=n_--n_+$ of a two-level system ($+$ for spin up and $-$ for spin down, S $=1/2$) is

$$\Delta n=\frac{w_{+-}-w_{-+}}{w_{-+}+w_{+-}+2R},\qquad(2)$$

where w_{+-} and w_{-+} are the relaxation probabilities from the state $+$ to $-$ and vice versa, and R is the EPR transition probability, which is proportional to the microwave power $P_{\mu W}$. The MCDA is proportional to the population difference Δn. Therefore, the microwave-induced change of the MCDA, i.e., the MCDA-EPR effect ($\Delta MCDA$), is proportional to $\Delta n(P_{\mu W}=0)-\Delta n(P_{\mu W}\neq0)$:

$$\Delta MCDA=MCDA(0)-MCDA(P_{\mu W})=\frac{c_1}{c_2}-\frac{c_1}{c_2+P_{\mu W}},$$

$$c_1\propto w_{+-}-w_{-+},$$

$$c_2\propto w_{-+}+w_{+-}.\qquad(3)$$

The parameters c_1 and c_2 were obtained for each transition from a fit of Eq. (3) to the measured relative intensities of the respective transitions at the three different microwave powers shown in Table I. Because of the long spin lattice relaxation time of the $\mathrm{As_{Ga}}$-X_2 defect at the measurement temperature of 1.5 K [$T_1=1/(w_{-+}+w_{+-})\approx2$ s], its EPR signals are saturated easily with the microwave power of 18 dBm. With no saturation the MCDA-EPR signal would be proportional to the microwave power [$\Delta MCDA\approx(c_1/c_2^2)\times P_{\mu W}$]. Saturation effects of the four allowed EPR transitions were already observed at a microwave power as low as -12 dBm. The intensity of the allowed transitions increased only by a factor of less than two when increasing the power by a factor of 1000 (from -12 dBm to 18 dBm). On the other hand, the forbidden transitions, which may have transition probabilities two orders of magnitude less than those of the allowed ones, increase linearly with the microwave power until they too are saturated. Therefore, the relative intensity of the allowed and forbidden transitions can be-

TABLE II. MCDA-EPR data of the $As_{Ga}-X_2$ defect at 1.5 K.

	hf interaction				
g_e factor	a_{hf} (MHz)	b_{hf} (MHz)	Quadrupole interaction q (MHz)	FWHM of hf lines $\Delta B_{1/2}$ (mT)	Spin lattice relaxation T_1 (s)
2.00 ± 1	2050 ± 30	<50	20 ± 5	45 ± 2	2.5 ± 0.5

come comparable under strong saturation, although the transition probabilities of allowed and forbidden transitions are very much different. Using Eq. (3) and the parameters c_1 and c_2 for As_{Ga}-X_2 at 1.5 K, it was shown that no saturation effects are expected for a microwave power of -48 dBm. However, in a measured spectrum with a microwave power of -48 dBm, the forbidden transitions could not be observed because of the small signal-to-noise ratio. Therefore, the relative line intensities of the allowed and forbidden transitions were calculated using Eq. (3) and the parameters c_1 and c_2 obtained from the fit described above. The calculated relative line intensities for -48 dBm are shown in the lowest row of Table I. These relative line intensities have the same ratio as the respective transition probabilities. The apparent microwave power dependence of the relative intensities of the forbidden lines in comparison to the allowed ones is caused by the saturation of the allowed transitions.

From the analysis of the calculated relative intensities of the forbidden lines at -48 dBm, where no saturation effects occur, we decomposed these intensities into a contribution that must be caused by a quadrupole interaction (no central line) and into another contribution that is probably caused by anisotropies or a large shf interaction. The ''outer'' forbidden lines with $\Delta m_S=\pm1$ and $\Delta m_I=\pm1$ at 794 mT and 945 mT (see Fig. 2) have almost double the intensity compared to the central one at 867 mT. The relative intensity of the central line at -48 dBm is a direct measure for the contribution of the forbidden transitions caused by anisotropies or by shf interactions (0.016). The relative intensities of the forbidden lines caused by a quadrupole interaction is the difference of the relative intensities of the outer forbidden and the central forbidden lines (0.014). Therefore, the value 0.014 represents the relative intensity of quadrupole-induced forbidden transitions in comparison to the allowed transitions.

From the spectral positions of the EPR transitions it cannot be decided whether a quadrupole interaction with a central nucleus exists. Only in higher order does the quadrupole interaction influence the line positions of the EPR transitions. Therefore, the quadrupole interaction of the central nucleus, if present, must be much smaller than the hf interaction. On the other hand, a quadrupole interaction influences the line intensities of the forbidden transitions as discussed above. Therefore, it is possible to estimate the quadrupole interaction indirectly via the relative intensities of the quadrupole-induced forbidden transitions in comparison to the allowed transitions. This procedure was performed using the value of 0.014 for the relative intensity of the quadrupole-induced forbidden transition without saturation and using Eq. (1). A quadrupole interaction parameter of $q/h\approx20\pm5$ MHz was estimated. A quadrupole interaction of the central As nucleus can only occur if the electric-field gradient at this position is not zero. From the quadrupole parameter q the field gradient was calculated to be approximately 3×10^{22} V m^{-2}. If the defect had tetrahedral symmetry (T_d), there would be no quadrupole interaction. Therefore, we conclude from the observation of the quadrupole-induced forbidden transitions in the MCDA-EPR spectrum that the As_{Ga}-X_2 defect must have a lower symmetry than T_d.

The relative transition probability of the forbidden transitions caused by anisotropies or a large shf interaction was estimated to be 0.016 compared to that of the allowed transitions (see Table I). It can be shown that the ratio of the respective transition probabilities caused by an anisotropic hf interaction roughly follows the square of the anisotropic hf interaction parameter b_{hf}, divided by the isotropic hf interaction parameter a_{hf}. If an anisotropy of the hf interaction would cause this part of the forbidden transitions (0.016), b_{hf} would be of the order of 200 MHz. On the other hand, no anisotropy of the MCDA-EPR spectrum of the As_{Ga}-X_2 defect was detected. An anisotropy of the hf interaction as small as 50 MHz would have been seen. Similar arguments can be applied for an anisotropy of the g tensor. Therefore, probably the large shf interactions of the first As shell of the defect ($\sim$250 MHz, see Sec. III B) are responsible for forbidden transitions with equal intensities for the outer and central lines. Numerical calculations of this effect showed that this is a reasonable explanation.[9] The data deduced from the MCDA-EPR results for the As_{Ga}-X_2 defect are collected in Table II.

B. MCDA-ENDOR measurements

MCDA-ENDOR was measured as a microwave- and rf-induced change of the MCDA. The magnetic field was set to the maximum of one of the hyperfine lines of the MCDA-EPR spectrum. MCDA-ENDOR lines were detected in the frequency range 12–40 MHz, 110–160 MHz, and 220–300 MHz. An MCDA-ENDOR spectrum over the whole frequency range is shown in Fig. 3 for B_0 30° off the [100] direction. A spectrum, measured in the high-frequency range (110–160 MHz) for the B$\|$[100] orientation, is reproduced in Fig. 4(a). The angular dependence of the MCDA-ENDOR lines was measured by rotating the crystal about a $\langle110\rangle$ axis from $B_0\|[100](0°)$ via $B_0\|[111](54.74°)$ to 70°. The signal-to-noise ratio of the measured ENDOR lines was very low, and it was difficult to follow a certain ENDOR line through the full angular dependence. Another problem, which complicated the analysis, was the overlap of many lines. In particular, a superposition of many ENDOR lines was observed in the high-frequency range [Fig. 4(a)].

The frequency positions of the MCDA-ENDOR lines can be calculated using the following Hamiltonian (S=1/2):

$$\mathbf{H}=\mu_B g\vec{\mathbf{S}}\cdot\vec{B}_0+\sum_i \vec{\mathbf{I}}_i\cdot\underline{\underline{A}}_i\cdot\vec{\mathbf{S}}-\sum_i g_{n,i}\mu_n\vec{\mathbf{I}}_i\cdot\vec{B}_0+\vec{\mathbf{I}}_i\cdot\underline{\underline{Q}}_i\cdot\vec{\mathbf{I}}_i, \tag{4}$$

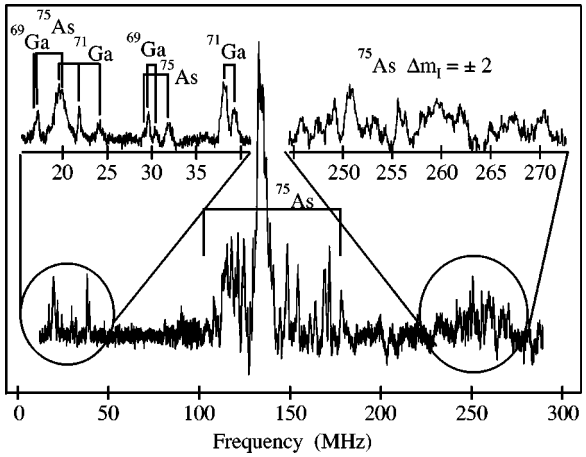

FIG. 3. MCDA-ENDOR spectrum of the As_{Ga}-X_2 defect at $T=1.5$ K. The photon energy was 1.287 eV, the magnetic field was 830 mT (see Fig. 2), the microwave frequency was 24.01 GHz, the angle between the static magnetic field and the [100] direction was 30° and between the [110] direction was 90°. The total time of measurement for this spectrum was 10 h.

where the first term is the electron Zeeman energy, the second is the shf interaction, the third is the nuclear Zeeman energy, and the fourth is the quadrupole interaction. $\underline{\underline{A}}_i$ is the shf tensor of the ith nucleus, $\underline{\underline{Q}}_i$ is the quadrupole tensor of the ith nucleus, μ_B is the Bohr magneton, g is the electron g value, $\vec{B}_0$ is the static magnetic field, $\vec{\mathbf{S}}$ is the electron spin operator, $\vec{\mathbf{I}}_i$ is the ith nuclear spin operator, μ_n is the nuclear magneton, and $g_{n,i}$ is the nuclear g-value of the ith nucleus. The frequencies for ENDOR transitions of the ith nucleus ν_i [selection rules for ENDOR: $\Delta m_{I,i}=\pm 1$, $\Delta m_{I,j}=0$ $(j\neq i)$, and $\Delta m_S=0$] are given in a first-order solution of the Hamiltonian as (see, e.g., Ref. 7):

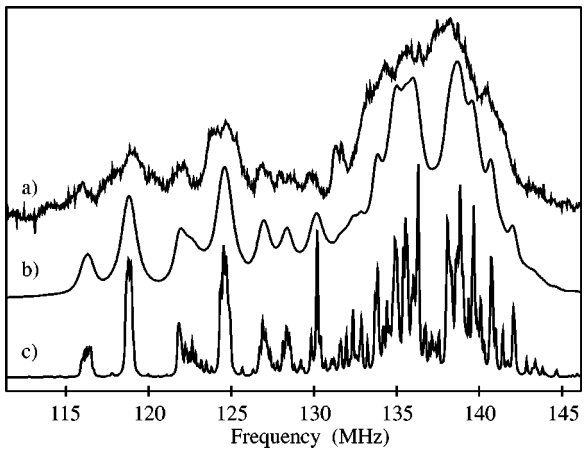

FIG. 4. (a) MCDA-ENDOR spectrum of the first As shell of the As_{Ga}-X_2 defect for the static magnetic field 5° off the [100] direction with the magnetic field at 725 mT (in the maximum of the lowest hf line), $T=1.5$ K, and photon energy of 1.287 eV. (b) Calculated spectrum with the parameters from Tables IV, V, and VI. The width of the lines was assumed to be 1 MHz, which was the width of the individual ENDOR lines found in the lower-frequency spectrum (12 to 40 MHz). (c) ''Stick spectrum'' of the calculated MCDA-ENDOR lines in which the relative line intensities reflect the transition probabilities. The width of the lines was set to 0.05 MHz.

$$\nu_i^{\pm}=\frac{1}{h}\left|m_{S,eff}W_{shf,i}+m_{q,i}W_{q,i}-g_{n,i}\mu_n B_0\right| \tag{5}$$

with

$$W_{shf,i}=a_i+b_i(3\cos^2\beta_i-1),$$

$$W_{q,i}=3q_i(3\cos^2\beta_i'-1), \text{ and}$$

$$m_{q,i}=\tfrac{1}{2}(m_{I_i}+m_{I,i}'), \tag{6}$$

where $m_{I,i}, m_{I,i}'$ are the quantum numbers of the nuclear levels associated with the ENDOR transitions and $m_{S,eff}$ is the effective spin quantum number. In the effective spin approximation the influence of internal fields like a strong hf interaction on the quantization of the electron spin is taken into account in first order. If a strong hf interaction is present, as observed here, the deviation of the effective spin quantum number $m_{S,eff}$ from $\pm 1/2$ is of the order of 10^{-2}. This deviation depends on the quantum number m_I of the central nucleus and, therefore, on which hf line the magnetic field was set during the ENDOR measurement. $W_{shf,i}$ is given in terms of the isotropic shf interaction constant a_i and the anisotropic shf interaction constant b_i. It is assumed that the deviation of the shf tensors from axial symmetry (b_i') is zero. For the quadrupole interaction, the parameter q_i is used (again axial symmetry is assumed, e.g., $q_i'=0$). The shf interaction and the quadrupole interaction parameters are related to the principal values of the shf and quadrupole tensors $\underline{\underline{A}}_i$ and $\underline{\underline{Q}}_i$ by $A_{xx,i}=a_i-b_i+b_i'$, $A_{yy,i}=a_i-b_i-b_i'$, $A_{zz,i}=a_i+2b_i$ and $Q_{xx,i}=-q_i+q_i'$, $Q_{yy,i}=-q_i-q_i'$, $Q_{zz,i}=2q_i$. β_i and β_i' are the angles between the static magnetic-field direction and the z axes of the principal axis systems of the shf—and quadrupole—tensor, respectively. ν_i^+ is the ''sum'' frequency where $m_S=-\frac{1}{2}$ and ν_i^- is the ''difference'' frequency where $m_S=+\frac{1}{2}$ (for details, see, e.g., Ref. 7, Chaps. 5 and 6).

The first step in the evaluation of the ENDOR data was to determine the chemical nature of the nuclei giving rise to the ENDOR lines. It can be seen from Eq. (5) that a specific ENDOR line will shift if the magnetic field B_0 is changed. Since the resonance condition for the EPR transition has to be fulfilled to measure ENDOR, the magnetic field can only be varied within the EPR linewidth. The chemical nature of nuclei giving rise to the ENDOR lines could thus be determined by observing the shift of ENDOR lines as a function of the magnetic field (for details see Ref. 7). The field shift experiment could be performed on all four hf lines of the EPR spectrum. The influence of the spin quantum state of the central nucleus (i.e., different $m_{s,eff}$ for different m_I's) on the shift could be neglected for the ENDOR lines in the low-frequency range. For these lines the additional shift due to the change in the effective spin quantum number $m_{S,eff}$ when changing from one hf line to another was smaller than the resolution of the field shift experiment. For the ENDOR lines around 130 MHz this effect prevented a chemical identification of the nuclei. If more than one hf-split EPR line was used for the magnetic-field shift experiment, the positions of the ENDOR lines could not be followed due to the superposition of too many lines. However, if the magnetic field was varied within the width of one individual hf EPR

line, the shift of the ENDOR lines was too small for an unambiguous identification. Only the sign of the slope of the shift could be determined. Besides the field shift experiment, ENDOR lines arising from Ga nuclei could be identified because the frequency positions of the ENDOR lines of the two Ga isotopes scale with the ratio of their nuclear g values $[g_n(^{71}\mathrm{Ga})/g_n(^{69}\mathrm{Ga}) = 1.27]$ if the quadrupole interaction can be neglected. The shf interaction and the nuclear Zeeman interaction are both proportional to the specific nuclear g value.

Figure 3 indicates the assignment of the ENDOR lines to specific nuclei surrounding the defect, i.e., ^{69}Ga, ^{71}Ga, and ^{75}As nuclei. No impurity neighbors were detected. The lines in the frequency range 110–160 MHz must be due to ^{75}As nuclei, although, it was not possible to identify the nuclei responsible for those lines with the field shift experiment as mentioned above. On the other hand, if the lines had been caused by Ga nuclei, the two Ga isotopes would have had to be seen. However, in that frequency range no pairs of ENDOR lines with a ratio of the frequency positions of 1.27 were observed. From the positive slope of the field shift of the ENDOR lines, we inferred that only the $m_S = -\frac{1}{2}$ branch (the ''sum'' frequency) was measured (assuming that $W_{shf} > 0$). It is often observed that only the sum frequency can be detected with ENDOR for a certain neighbor shell. The complex relaxation behavior of the electron-nuclear spin system is probably responsible for this effect.

The ENDOR signals in the highest-frequency range (240–280 MHz) must be due to higher-order transitions, otherwise, the shf interaction causing these lines would be ~500 MHz. A shf interaction of about 500 MHz is not consistent with the individual linewidth of the four hf lines of the EPR spectrum. A shf interaction of only one nucleus (As or Ga) with 500 MHz would cause a linewidth of more than 50 mT. However, the measured linewidth is only 45 mT. With the assumption that $\Delta m_I = \pm 2$ ENDOR transitions of the As nuclear spins are responsible for the lines in the range 110–160 MHz, the high-frequency lines can be explained. We conclude that the lines around 130 MHz (and those around 260 MHz) are due to the first ^{75}As shell since it is expected that the nearest-neighbor shell of a defect will have the highest shf interaction.

The lines in the low-frequency range (14–40 MHz) must be due to more distant Ga and As nuclei with the As lines in this low-frequency range due to a higher arsenic shell (see Fig. 3). For an As interstitial, it would be expected that the shf interactions of the As and Ga nuclei in the nearest neighborhood would be the same order of magnitude. However, some As-ENDOR lines were at a much higher frequency than any Ga-ENDOR lines. Hence, the shf interactions of the As nuclei causing the high-frequency lines must be much larger than those for the gallium. We conclude that the defect has only As atoms in the nearest-neighbor shell and, thus, must be As_{Ga} related and not an As interstitial.

For the structural analysis of the As_{Ga}-X_2 defect, the MCDA-ENDOR spectrum in the frequency range 110–160 MHz [see Fig. 4(a)] is very important. It yields information about the nearest (first) As shell and, therefore, information about the symmetry of the defect. Because of effects of pseudodipolar coupling[10,11] it was not possible to precisely analyze the angular dependence of the As lines in the 110–160 MHz range. However, even a crude estimate of the shf interactions together with the measured EPR linewidth suffices to decide on the number of equivalent nearest As neighbors and thus determine the most important structural feature. Therefore, the analysis of the first As shell took place in a three-step process. First the shf interaction of this shell was estimated in a first-order approximation. Then, an EPR lineshape analysis was performed with the estimated shf interaction of the first As shell used to decide on the number of the equivalent neighbor nuclei of this shell. In the last step a full diagonalization and a spectral analysis of the ENDOR spectrum for the magnetic field parallel to the [100] direction was performed to get a more precise estimate of the shf and quadrupole parameters of the first As shell.

The linewidth of an inhomogeneously broadened EPR line of a paramagnetic defect can be calculated using the shf interactions of the neighbor nuclei (see, e.g., Ref. 7). For this linewidth calculation we only took into account a crude estimate of the shf interaction in the following way. From Fig. 4(a), we estimated W_{shf} of the nearest As shell for the [100] direction of the magnetic field using Eq. (5). In this first-order estimate we made crude assumptions on the symmetry. For B_0 parallel to the z axis, assumed to be the [100] direction, the shf interaction would be ~250 MHz. If the defect had tetrahedral symmetry, the first As shell would consist of four equivalent As atoms. In order to obtain a smooth envelope curve for the calculated MCDA-EPR line as found in the experiment (Fig. 1), a minimum width of 7 mT was chosen for each individual As shf line. The additional broadening of the EPR line from higher shells is taken into account by this individual width of each As shf line. The half width of the calculated EPR line, assuming four equivalent As neighbors having a shf interaction of 250 MHz each and taking the smallest possible individual linewidth of 7 mT, is 53 mT (full width at half-maximum). This value is the lowest limit of the half-width under the assumption of four equivalent As neighbors. It is large compared with the measured linewidth of (45 ± 2) mT. The assumption of three equivalent As nuclei in the first shell gives a half-width of approximately 44 mT, which is in better agreement with the experiment. The result for two nuclei in the first As shell is 36 mT. This is too small. Thus, we conclude that the first As shell consists of three nuclei.

The highest symmetry of a defect with three As nuclei in its first shell is trigonal (C_{3v}). It cannot be ruled out that the symmetry is lower (C_{1h}). In the following, we assume trigonal symmetry. Then, there are four defect orientations, corresponding to each of the four ⟨111⟩ directions. The splitting of the first two As shells around a Ga site into subshells when the symmetry is lowered from tetrahedral to trigonal is described in Table III. The shf and quadrupole tensors of the As nuclei of the first As shell have monoclinic symmetry (for short: the first As shell has monoclinic symmetry). The z and the x axes of the principal axes systems of the shf and quadrupole tensors of this monoclinic shell must be located in a (110) plane that contains the As_{Ga} nucleus and the ''distorted'' fourth As site. Figure 5 shows the two subshells [I_a and I_b] for the first As shell for the two trigonally symmetry defect models proposed by v. Bardeleben and co-workers.[3,6] Three Euler angles (α,β,γ) are necessary to describe the orientation of such a tensor. Because of the orientation of the z

TABLE III. The splitting of the neighbor shells into subshells around a Ga lattice site, if the symmetry is lowered from tetrahedral (T_d) to trigonal (C_{3v}).

	Lattice	Tetrahedral		Trigonal		
Atom	Distance (Å)	Number of nuclei	Symmetry	Number of nuclei	Symmetry	Symbol
As	2.45	4	trigonal	3	monoclinic	I_a
				1	trigonal	I_b
Ga	3.99	12	monoclinic	3	monoclinic	II_a
				6	triclinic	II_b
				3	monoclinic	II_c
As	4.68	12	monoclinic	3	monoclinic	III_a
				3	monoclinic	III_b
				6	triclinic	III_c

and x axes of the principal systems of the tensors, two of the Euler angles (α and γ) are not free parameters. β is the angle between the z axis of the principal system of an interaction tensor and the [100] direction. $\beta = 54.74°$ for the first As shell would mean that the z axes of the respective tensors would exactly point to the Ga lattice site on which the As_{Ga} atom would be located if the defect had T_d symmetry. A deviation from this angle indicates a distortion of the defect from T_d.

The large shf interaction ($\sim$250 MHz) causes higher-order effects, which produce additional splittings. If the three nuclei in the shell are equivalent, which is the case for $B_0 \| [100]$, the pseudodipolar coupling is important. The nuclei interact with each other via the electron spin. The spin state of a specific nucleus influences the quantization axis of the electron spin. This changes the shf interaction with other equivalent nuclei. The pseudodipolar coupling produces a multiplet structure for each ENDOR line. If a quadrupole interaction is not considered, this multiplet structure is determined by the total nuclear spins I_g that are combined from the individual nuclear spins of the equivalent nuclei. The splitting within this structure is of the order of $2W_{shf}^2/(\mu_B g B_0)$. For three equivalent nuclei each with a spin of 3/2, the maximum total spin is $I_{g,max} = 9/2$. Allowed ENDOR transitions can take place within this $I_{g,max}$ manifold. Therefore, $2 \times I_{g,max} = 9$ allowed lines are expected. The relative intensity of these lines depends on the statistical weights of the different possibilities to combine to a specific total spin I_g and on the relative probabilities of the different transitions within the manifolds of the I_g values. If a quadrupole interaction is present, the situation is much more complicated. Another complication is the fact that forbidden transitions can become quasiallowed due to the pseudodipolar coupling effects. For further details, the reader is referred, for example, to Refs. 10 and 11.

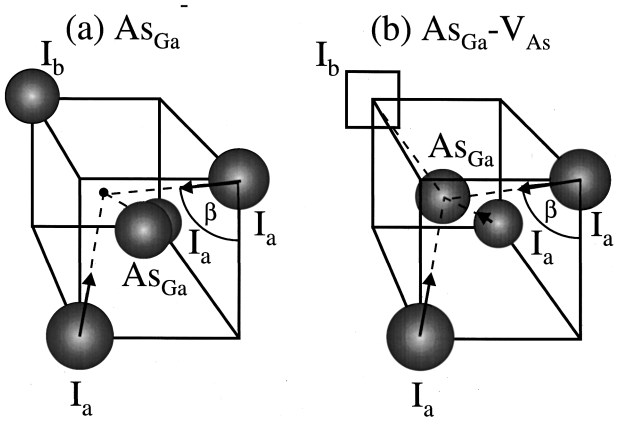

FIG. 5. The two different models for the As_{Ga}-X_2 defect. (a) The distorted As_{Ga}^- (Ref. 6), where the As_{Ga} atom is moved along the [111] direction towards the interstitial position (planar As configuration). (b) The As_{Ga}-V_{As} with an As vacancy [I_b] in the next-neighbor shell (Ref. 3). The As_{Ga} atom is relaxed towards the As vacancy. The arrows indicate the direction of the z axes of the principal systems of the shf tensors of the three equivalent As neighbors. They point to a location 20–30 % of the bond length off the regular As_{Ga} position. For the As_{Ga}-V_{As} model it was assumed that the As_{Ga} atom is relaxed to this point. The angle β (see Table IV) was assumed to be 70° as determined from experiment. $\beta = 54.74°$ for As_{Ga} on a regular lattice position.

For the calculation of the spectrum (Fig. 4), neither Eq. (5) nor the effective spin approximation, where the electron spin operator in the Hamiltonian [Eq. (4)] is replaced by the effective electron spin and the nuclear spins are assumed to be independent from each other, is sufficient. In the effective spin treatment of the Hamiltonian, the diagonalization is only performed for the ''reduced'' nuclear spin matrices. Because of the large shf interactions of the three As nuclei (about 250 MHz), the full matrix including the electron spin and the three As nuclear spins of the spin Hamiltonian had to be diagonalized. The influence of the hf interaction on the MCDA-ENDOR spectrum was neglected. It produces a shift that is equal for the ENDOR lines of each m_S branch. In the ENDOR experiment the magnetic field B_0 is set to one specific hf-split EPR line. Therefore, all measured defects have

TABLE IV. shf interactions of the neighbor shells, I_a, $II_{c,b}$, and III_b. The As atoms of shell III_b are those near to the As vacancy. The Ga atoms of shell II_c are those nearer the vacancy, those of II_b the one in the plane of the As_{Ga}.

	Shell	a/h (MHz)	b/h (MHz)	Symmetry
1.	^{75}As-shell (I_a)	252±5	24±5	monoclinic
2.	^{75}As-shell (III_b)	47.6±0.1	1.65±0.05	monoclinic
1.	^{69}Ga-shell (II_c)	42.3±0.1	1.4±0.05	monoclinic
2.	^{69}Ga-shell (II_b?)	≈17	≈0.6	triclinic

TABLE V. Euler angles orientations of the shf tensors.

	Shell	α[a] (degrees)	β[b] (degrees)	γ[c] (degrees)	Symmetry
1.	As shell (I_a)	0	70 ± 5	45	monoclinic
2.	As shell (III_b)	0	0 ± 2	45	monoclinic
1.	Ga shell (II_c)	0	40 ± 2	45	monoclinic
2.	Ga shell (II_b?)	?	?	?	triclinic

[a]The z and the x axes of the principal systems of the shf tensors of the monoclinic shells must be located in a (110) plane which contains the As_{Ga} nucleus and the distorted fourth As site. Therefore, the angles α and γ of these shells are not free parameters.

[b]β is the angle between the z axis of the principal system of the shf tensor and the [100] direction. $\beta = 54.74°$ for the first As shell would mean that the system is not relaxed (for example, a system with T_d symmetry).

[c]See note a.

the same quantum number m_I of the spin of their central nuclei. The spectrum of Fig. 4(a) was recorded on the low-field EPR line (725 mT). For this line the shift due to the hf interaction is 1.4%. The result of this shift is that the shf parameters obtained from a fit of the $m_S = -1/2$ branch are reduced by 1.4%.

The matrix of the spin Hamiltonian for the first As shell has a dimension of 128 (three nuclear spins of 3/2 and one electron spin of 1/2). The matrix consists of two subsystems for each m_S branch. Within such a subsystem with a dimension of 64, ENDOR transitions are possible. That leads to a number of $\binom{64}{2} = 2016$ transitions for each subsystem. Because we only measured the sum frequency (see above), we have to consider 2016 transitions. From our calculations, it turned out that most of them have a negligible transition probability, e.g., are forbidden transitions.

First, the shf and quadrupole parameters of the first As shell were estimated by a least-squares fit of the angular dependence of the MCDA-ENDOR lines with the approximation of an effective electron spin.[7] Then, the parameters were determined by the ''best'' fit of the calculated spectrum to the experimental spectrum with the full diagonalization of the Hamiltonian. In Fig. 4(b) the calculated MCDA-ENDOR spectrum for $B_0 \| [100]$ with the shf and quadrupole interaction parameters from Tables IV, V, and VI (first As shell) is shown. The MCDA-ENDOR spectrum in Fig. 4 is a superposition of several hundred lines! A linewidth of 1 MHz for each MCDA-ENDOR line was assumed. This width is a reasonable value for the MCDA-ENDOR lines in GaAs. It was measured in the low frequency range where the pseudodipolar coupling can be neglected. The frequency positions of the individual MCDA-ENDOR lines are illustrated in Fig. 4(c) (stick spectrum).

For the analysis of the ENDOR lines in the lower-frequency range 12 to 40 MHz (higher shells), we kept the assumption of trigonal symmetry. In Table III, it is shown that the second As shell of a defect on the Ga sublattice with T_d symmetry splits into the subshells III_a, III_b, and III_c when the symmetry is lowered to C_{3v}. From the angular dependence it is not possible to unambiguously assign the ENDOR lines arising from As nuclei in the low-frequency range to one of these subshells. We attributed these arsenic ENDOR lines to the monoclinic subshell III_b. Under this assumption, the z axes of the principal systems of the shf tensors of this subshell would be oriented parallel to the $\langle 100 \rangle$ directions ($\beta = 0°$) and would point to the lattice site I_b. This assumption will be justified in the discussion in the next section about the spin density distribution. We assigned the observed Ga ENDOR lines to the monoclinic subshell II_c and tentatively to the subshell II_b, for which the interaction parameters could only roughly be estimated. No quadrupole interaction was observed within experimental error. The shf parameters are collected in Tables IV and V.

Using the shf parameters for all measured shells for the [100] orientation of the static magnetic field, the EPR linewidth was recalculated. The resulting half-width with three As nuclei in the first As shell is 46 mT. This is in very good agreement with the measured width of (45 ± 2) mT. If the linewidth is calculated with three As nuclei in the first shell, the linewidth is not noticeably increased by taking into account an additional fourth As nucleus (on the ''distorted'' fourth As site) with a shf interaction up to 120 MHz. This nucleus if present on site I_b would show a trigonal angular dependence of its ENDOR lines, which was, however, not observed.

IV. DISCUSSION

The main result of our ENDOR analysis is that the As_{Ga}-X_2 defect has a trigonal C_{3v} or the lower C_{1h} symmetry and that there are only three As nuclei with a large shf interaction ($\sim$250 MHz) in the first shell. These results are consistent with the two models of paramagnetic As antisite-related defects: the As_{Ga}-V_{As} and the isolated but distorted $As_{Ga}{}^{-}$. Both models were proposed by v. Bardeleben and co-workers[3,6] and are shown in Fig. 5.

In the model of a distorted $As_{Ga}{}^{-}$ defect, the central As_{Ga} nucleus is moved to an off-center position along the [111] direction towards the interstitial position because the bond between the As_{Ga} and I_b atom is assumed to be broken, i.e.,

TABLE VI. Quadrupole parameters of the first As shell.

q/h (MHz)	q'/h (MHz)	α[a] (degrees)	β (degrees)	γ (degrees)
0.9 ± 0.3	0 ± 0.3	0	165 ± 5	45

[a]For the definition of the Euler angles see the notes in Table V.

missing an electron [see Fig. 5(a)]. This means there are three equivalent As neighbors [labeled with I_a in Fig. 5(a)] and that the fourth As neighbor (labeled I_b) should have only a very small shf interaction. The shf interaction tensor of this fourth As neighbor would have trigonal symmetry. The z axis of the principle system of the shf tensor would point along the [111] direction towards the As_{Ga} atom. This fourth As nucleus with trigonal symmetry (I_b) must have a shf interaction not larger than 120 MHz, as shown by the EPR linewidth analysis. The ENDOR lines of an As nucleus up to a maximum shf interaction of 120 MHz are expected to be below 70 MHz. A careful search for ENDOR lines with trigonal symmetry (having a maximum frequency in the [111] directions) failed to detect As ENDOR lines below 70 MHz.

Another argument against the model of the distorted As_{Ga}^- is the orientation of the shf tensors of the three equivalent As neighbors of the first shell (I_a). From Table V it can be seen that the angle β of the shf tensor has a value of 70°. A larger angle than 54.74° indicates that the z axes of the principle systems of the shf tensors of the first As shell (I_b) point to a location between the regular As_{Ga} position (Ga site) and the I_b site. If the angle is smaller than 54.74°, the z axes would point to a location between the regular As_{Ga} position and the interstitial site. The z axes of the shf tensors of the first As shell point to the center of the spin density distribution. Since $\beta \approx 70° > 54.74°$, it is inferred that this center of spin density distribution must be located between the regular As_{Ga} position and the lattice site I_b. For a distorted As_{Ga}^- defect this is a region of low spin density, since the bond between the As_{Ga} atom and the fourth As neighbor I_b is broken. Thus, the large β value does not favor the As_{Ga}^- model.

A model, which reasonably explains all ENDOR data, is the As_{Ga}-V_{As} an As_{Ga} with an As vacancy in the first As shell. This model is shown in Fig. 5(b). From now on, we shall refer to the defect as As_{Ga}-V_{As}. From calculations of the spin density distribution of the unrelaxed As_{Ga}-V_{As} defect in its paramagnetic charge state, it was concluded that this configuration has the character of the As vacancy (V_{As}).[12] Most of the spin density would be located at the vacancy. After the introduction of a relaxation of 30% of the bond length of the As_{Ga} nucleus towards the As vacancy, the highest spin density would appear at the As_{Ga}.[12] No relaxations of the neighbor atoms were considered. If we assumed that the As_{Ga} atom is located at the center of the spin density, the deviation of the shf tensor angle β of the first As shell would indicate a relaxation of the As_{Ga} atom towards the As vacancy of about 20–30% of the bond length. This would be in excellent agreement with the calculations of Delerue.[12] On the other hand, if the total measured spin density is calculated from our shf data within the linear combination of atomic orbitals (LCAO) approximation; see Ref. 13, the hf and shf interactions can account for only 50% of the spin density. Most of this spin density is located at the As_{Ga} atom and its three As neighbors (14% at the As_{Ga} atom and 27% at the three As neighbors). It is possible that a large amount of spin density is located in the As vacancy, which we cannot measure with ENDOR. This would mean that the As_{Ga} atom is not the center of spin density and the relaxation of the As_{Ga} atom cannot be estimated from the shf tensor angles of the first As shell. A further indication of this situation is the orientation of the shf tensor angles of the As shell III_b. In our assignment of the ENDOR lines to the As shell III_b, the z axes of the principle systems of the shf tensors of this shell point to the As vacancy. This would indicate that a substantial spin density is located at the As vacancy.

Another calculation was carried out by Poykko *et al.*[14] for the diamagnetic $(As_{Ga}\text{-}V_{As})^+$ state. There the relaxations of the neighbor atoms were taken into account. Unfortunately, it was not possible to calculate the neutral paramagnetic state with their method. For the positive charge state, they found several stable configurations of the defect. Besides the $(As_{Ga}\text{-}V_{As})^+$, which turned out to be the most stable one, they found the V_{Ga}^+ and the $(V_{GaAs}\text{-}As_i)^+$ configuration to be stable. The $(As_{Ga}\text{-}V_{As})^+$ would have trigonal symmetry (C_{3v}) even if neighbors are allowed to relax. A relaxation of the As_{Ga} nucleus of 12% towards the V_{As} was calculated.

According to Ref. 14, the states of the $(As_{Ga}\text{-}V_{As})^0$ defect can be created by a hybridization of the states of the double vacancy V_{GaAs} with an As atom. In this picture the unpaired electron of the neutral state occupies an a_1 state. Therefore, no spontaneous lowering of the C_{3v} symmetry is expected. It is known that the isolated As_{Ga} defect is paramagnetic in its singly positive charge state and that the spin density at its As_{Ga} atom is approx. 18% as calculated in Ref. 1. Therefore, it can further be assumed that the As_{Ga} of the neutral complex bears a positive charge (spin density at the As_{Ga} atom is 14%), whereas the V_{As} is negatively charged. With this model the quadrupole interaction of the As_{Ga} nuclear spin, estimated from the occurrence of the forbidden EPR transitions, can be qualitatively understood.

A rough estimate for the quadrupole interaction of the central As_{Ga} nucleus, caused by an elementary charge, is given by the following equation (see, e.g., Ref. 7):

$$q = \frac{e^2 Q(1-\gamma_\infty)}{2I(2I-1)4\pi\epsilon_0 R^3}, \tag{7}$$

where Q is the quadrupole moment of the nucleus, e is the elemental charge, ϵ_0 is the electrical field constant, R is the distance of the nucleus from the point charge, and $(1-\gamma_\infty)$ is the Sternheimer anti-shielding factor for a charge outside the core of the atom. $(1-\gamma_\infty)$ is 40 for As.[15] For a point charge of one and $q = 20$ MHz as estimated experimentally, a distance of 60% of that between the unrelaxed As_{Ga} atom and the As vacancy was calculated. This would favor the assumption that the As_{Ga} atom is relaxed towards the V_{As} [see Fig. 5(b)].

A further reason for a quadrupole interaction may be the electric-field gradient arising from the unpaired spin density moving in a p orbital only:[16]

$$q(P_\sigma) = \frac{Se^2 Q(1-\gamma)}{2I(2I-1)\epsilon_0\mu_0 g_e g_N \mu_B \mu_N} b(P_\sigma), \tag{8}$$

where $(1-\gamma)$ is the atomic antishielding factor, which is not known and which is expected to be approximately one, μ_0 is the magnetic induction constant, S is the electron spin, and $b(P_\sigma)$ is the anisotropic hf parameter without contributions from a point dipole-dipole interaction b_{dd}. The maximum anisotropy of the hf interaction which would not be resolved

in the MCDA-EPR spectrum from an angular dependence would be about 50 MHz (this corresponds to a total splitting of the hf quartet of 4.5 mT). An estimate of the maximum quadrupole interaction $q(P_\sigma)$ with $b(P_\sigma)=50$ MHz gives a value of only 3 MHz. Therefore, the main contribution to the quadrupole interaction must arise from a charged constituent in the neighborhood of the As_{Ga} nucleus like the negatively charged vacancy in the $As_{Ga}{}^{+}$-$V_{As}{}^{-}$ configuration.

V. CONCLUSIONS

The As_{Ga}-related defect produced by electron-irradiation in *n*-type GaAs was investigated with MCDA-EPR/ENDOR techniques. From the MCDA-EPR spectrum it was shown that the defect has a central As atom. The microwave power dependence of the MCDA-EPR spectrum was explained with forbidden quadrupole-induced transitions of the As_{Ga} nucleus. A quadrupole interaction of the central As_{Ga} nucleus, which is not directly resolved in the MCDA-EPR spectrum, was estimated to be $q=20\pm5$ MHz from the relative intensity of these forbidden MCDA-EPR transitions. From the existence of this quadrupole interaction, it was further concluded that the defect symmetry is lower than T_d. With MCDA-ENDOR measurements the shf interaction of the first As shell was resolved. This shf interaction is only consistent with the MCDA-EPR linewidth, if three As neighbors are assumed, supporting the results from the EPR power dependence that the symmetry is lower than T_d. It is concluded that the As_{Ga}-related defect is not the distorted $As_{Ga}{}^{-}$ because the fourth As neighbor was not found and because a high spin density was found in a region where a low spin density would be expected. All observations are consistent with the model of an arsenic antisite with an arsenic vacancy in the nearest-neighbor position (As_{Ga}-V_{As}). There is evidence for a relaxation of the As_{Ga} atom towards the V_{As}. This would be in agreement with theory. The quadrupole interaction of the central nucleus was estimated to be consistent with a charge distribution where a positive charge is located at the As_{Ga} nucleus and a negative charge is located at the V_{As}.

ACKNOWLEDGMENTS

Support by the Deutsche Forschungsgemeinschaft is gratefully acknowledged. The authors also gratefully acknowledge the use of the electron accelerator ELIAS at the Forschungszentrum Jülich to electron irradiate the samples.

[1] J.-M. Spaeth and K. Krambrock, in *Advances in Solid State Physics*, edited by R. Helbig (Vieweg, Braunschweig/Wiesbaden, 1993), Vol. 33, p. 111.

[2] J.-M. Spaeth, D. M. Hofmann, and B. K. Meyer, in *Microscopic Identification of Anion Antisite Defects in GaAs by Optically Detected Magnetic Resonance*, MRS Symposia Proceedings No. 46 (Materials Research Society, Pittsburgh, 1985), p. 185.

[3] H. J. von Bardeleben, J. C. Bourgoin, and A. Miret, Phys. Rev. B **34**, 1360 (1986).

[4] K. Krambrock, Ph.D. thesis, Paderborn, Germany, 1992.

[5] H. J. von Bardeleben, A. Miret, H. Lim, and J. C. Bourgoin, J. Phys. C **20**, 1353 (1987).

[6] H. J. von Bardeleben, C. Delerue, and D. Stievenard, Mater. Sci. Forum **143-147**, 223 (1994).

[7] J.-M. Spaeth, J. R. Niklas, and R. H. Bartram, in *Structural Analysis of Point Defects in Solids*, edited by M. Cardona, P. Fulde, K. von Klitzing, and H.-J. Queisser, Springer Series in Solid-State Sciences Vol. 43 (Springer-Verlag, Heidelberg, 1992).

[8] A. Abragam and B. Bleaney, *Electron Paramagnetic Resonance of Transition Ions* (Dover, New York, 1986).

[9] F. Wirbeleit and J. R. Niklas (private communication).

[10] T. E. Feuchtwang, Phys. Rev. **126**, 1628 (1962).

[11] H. Seidel, Habilitation thesis, Stuttgart, 1966.

[12] C. Delerue, Phys. Rev. B **44**, 10 525 (1991).

[13] G. D. Watkins and J. W. Corbett, Phys. Rev. **121**, 1001 (1961).

[14] S. Poykko, M. J. Puska, M. Alatalo, and R. M. Nieminen, Phys. Rev. B **54**, 7909 (1996).

[15] D. Gill and N. Bloembergen, Phys. Rev. **129**, 2398 (1963).

[16] J. Owen and J. H. M. Thornley, Rep. Prog. Phys. **29**, 675 (1966).